Title: The host brain is permissive to colonization by *Toxoplasma gondii*

Authors: Wincott, CJ.[1], Sritharan, G.[1,2], Bunyan, M.[3], Alves, E.[1], Benns, HJ.[1,4], Frickel, EM.[3,5], Ewald, SE.[6], Child, MA.[1*]

* indicates corresponding author

Author affiliations:

[1] Department of Life Sciences, Imperial College London, South Kensington Campus, London SW7 2AZ, UK

[2] Department of Biological Sciences, Birkbeck, University of London, Malet Street, Bloomsbury London WC1E 7HX, UK

[3] Host-Toxoplasma Interaction Laboratory, The Francis Crick Institute, 1 Midland Road, London NW1 1BF, UK

[4] Department of Chemistry, Imperial College London, White City Campus, London W12 0BZ, UK

[5] Institute of Microbiology and Infection, School of Biosciences, University of Birmingham, Edgbaston B15 2TT, UK

[6] Department of Microbiology, Immunology and Cancer Biology at the Carter Immunology Center, University of Virginia School of Medicine, Charlottesville VA 228908 USA

Summary

Pathogenic infections and the diseases they cause are defined by invasion and colonization of distinct host cell types and tissue niches. In the case of viruses and bacteria, molecular and cellular barcoding has shaped our understanding of within-host pathogen population dynamics, and informed therapeutic intervention strategies. Host brain colonization is a clinically untreatable feature of persistent infection by the eukaryotic pathogen *Toxoplasma gondii,* and the process remains poorly understood. The host blood-brain barrier is expected to physically restrict parasite colonization of this tissue niche and force the infection through a selection bottleneck, however tools and technologies to test this hypothesis have not been available. Here, we have developed a simple CRISPR-based method to barcode *Toxoplasma* parasites, and then used complex libraries of barcoded parasites to define how the different phases of an infection shape the pathogen population structure. Unexpectedly, we have discovered that the murine host brain does not restrict parasite colonization, with the population structure predominantly shaped by a bottleneck experienced during the acute phase of infection. These data support an evolutionary strategy to maximize genetic diversity of parasite persister cells within the intermediate host brain for subsequent transmission into the definitive feline host.

Main text

Microbial colonization of tissues and organs within the host organism is a key feature of host-pathogen interactions, and often responsible for the pathology of the associated disease (Ribet and Cossart, 2015). For example, colonization of the brain by the eukaryotic protozoan parasite *Toxoplasma gondii* during the chronic phase of an infection can lead to toxoplasmic encephalitis in immunocompromised hosts (Luft et al., 1993). The spatial redistribution of a *T. gondii* infection as it transitions from the broadly distributed acute to the skeletal muscle and brain-associated chronic phase is accompanied by cellular differentiation; the parasite converts from the tachyzoite to the slower growing encysted bradyzoite (Wohlfert et al., 2017). Bradyzoite differentiation in niches like the brain is essential for transmission, and therefore competition prior to and during brain colonization is expected to have an impact on long-term success of a clone. Significant advances have been made in understanding how tachyzoites differentiate into persister-like bradyzoites (Barrett et al., 2019), with the transcription factor BFD1 recently shown to be a master developmental regulator (Waldman et al., 2020). In contrast, the effect of this developmental transition upon

62 the parasite's population structure during colonization of the immune-privileged brain niche remains an
63 intangible mystery. One critical function of the blood-brain-barrier (BBB) is to physically restrict the access
64 of pathogens such as *T. gondii* to the brain (Kim, 2008, Elsheikha and Khan, 2010). Therefore, it is
65 anticipated that the BBB imposes a selection bottleneck upon the *T. gondii* population as the chronic
66 infection is established, but we lack the tools to determine if this is true.

67 DNA-based molecular barcoding has been instrumental for understanding how the host and the
68 infection process influences genetic complexity of pathogen populations, and colonization dynamics
69 (Blundell and Levy, 2014, Kebschull and Zador, 2018). Early studies using restriction site-tagged poliovirus
70 identified a bottleneck limiting the genetic diversity of viral quasispecies transmitted to the murine brain
71 (Pfeiffer and Kirkegaard, 2006). Furthermore, studies using Wild-type Isogenic Tagged Strains (WITS) of
72 *Salmonella* have provided key insights into selection bottlenecks experienced during colonization of distinct
73 tissues and organs across the different phases of the infection (Grant et al., 2008, Lim et al., 2014). The
74 population structure of *Salmonella* infection was found to experience dramatic selective bottlenecks during
75 the colonization of the gut niche, with predominant colonizing strain also the dominant strain transmitted by
76 super shedders (Lam and Monack, 2014). The generation of WITS requires the insertion of molecular
77 barcodes into the genome of the infectious agent (Grant et al., 2008). These cellular barcodes then function
78 as neutral alleles, allowing the complexity of the population to be closely monitored and mapped over the
79 course of an infection using quantitative next-generation sequencing (NGS) approaches. Molecular
80 barcoding has provided unique insights into the population structures of both viral and prokaryotic infectious
81 disease, but due to technical limitations has not been used to study the within-host population structure of
82 eukaryotic pathogens.

83 Here, we define how the acute-to-chronic transition and brain colonization by *T. gondii* shapes the
84 active infection population structure of this eukaryotic pathogen. We establish a simple, scalable CRISPR-
85 based single-strand oligo recombineering strategy to efficiently generate libraries of molecularly barcoded *T.*
86 *gondii* strains. In the absence of environmental pressures these barcode libraries are stable, enabling
87 quantitative analysis of the effect of the intact host organism environment upon parasite population
88 dynamics. We then use these libraries to investigate the influence of the host organism upon the infection
89 population structure of *T. gondii,* revealing that the brain niche is unexpectedly permissive to colonization by
90 this ubiquitous pathogen.

91

92 **Results**

93 ***Toxoplasma tachyzoites can be molecularly barcoded with a simple CRISPR-based strategy***

94 Inspired by WITS (Grant et al., 2008), we first sought to establish a system to molecularly barcode the
95 eukaryotic pathogen, *T. gondii*. A CRISPR-Cas9 single-strand oligonucleotide recombineering strategy was
96 designed for site-specific integration of molecular barcodes into the genome of *Toxoplasma* tachyzoites (**Fig.**
97 **1a**). Parasites lacking the non-homologous end joining pathway (Huynh and Carruthers, 2009) (RHΔ*ku80*)
98 were co-transfected with a single plasmid encoding both the Cas9 nuclease and guide RNA (gRNA) scaffold
99 (Shen et al., 2014), and a unique single-stranded oligo donor template encoding the molecular barcode.
100 Targeting of the Cas9 nuclease to the *UPRT* locus promoted efficient integration of a 60-nucleotide single-
101 stranded donor template. Barcode integration disrupted the *UPRT* coding sequence, conferring resistance to
102 the prodrug 5-fluorodeoxyuridine (FUDR) and enabling positive selection of successfully barcoded parasite
103 strains (Donald and Roos, 1995). Our strategy also deleted both the protospacer DNA sequence recognized
104 by the CRISPR gRNA and the protospacer adjacent motif (PAM), preventing further modification of the site
105 following a single barcode integration event. Sanger sequencing of an amplicon derived from the *UPRT*
106 locus in the drug-resistant parasite population confirmed the expected genomic rearrangement following
107 barcode oligo integration (**Fig. 1b**). This demonstrated that individual parasites encode single barcodes
108 within amplicons derived from the *UPRT* locus, and validated the use of short single-stranded donor
109 templates for HDR in *Toxoplasma*. This strategy allows for unique single barcodes to be inserted at the same
110 genomic position, enabling population genetic studies.

111

112 ***Barcode alleles can be identified and quantified in complex populations***

113 Following successful design and implementation of our molecular barcoding strategy, a multiplexed
114 platform was established for 96-well plate-based transfections. This enabled parallel production of plate-
115 mapped 96-member libraries of molecularly barcoded parasites. To quantify the relative representation of
116 individual barcodes within a complex 96-member library pool we employed an NGS pipeline based on
117 amplicon deep sequencing of the barcoded *UPRT* locus, combined with barcode counting (Smith et al.,
118 2009) (**Fig. 1c**). A specific amplicon encompassing the molecular barcode was amplified from parasite
119 genomic DNA (**Fig. S1**). The purified amplicon was indexed and sequenced on an Illumina platform (MiSeq

120 or NextSeq), and the data processed using Galaxy (Afgan et al., 2018). We first tested our ability to identify
121 all 96 variants within a single population. Following multiplexed transfections, all 96 uniquely barcoded
122 strains were combined to create a mixed library pool and then processed within our pipeline. We
123 successfully identified all 96 uniquely barcoded strains (**Fig. 1d**). Biological replicates of our multiplexed
124 transfections, and technical replicates with unique NGS libraries prepared from the same genomic material
125 were compared (**Fig. S2a**). We observed the highest variation between independent biological experiments
126 (**Fig. S2b**). Independently indexed libraries generated from single genomic samples were well correlated
127 with the relative representation of individual barcodes within complex populations, indicating excellent
128 technical reproducibility (**Fig. S2c and d**).

129 To determine the sensitivity of the NGS readout we defined the relationship between parasite
130 number, barcode frequency within the complex population, and NGS reads. Using a plate-based two-fold
131 dilution series of the barcoded strain library followed by NGS and barcode counting, we observed a positive
132 correlation between parasite input and read output from 10,000 parasites/barcode down to a lower limit of
133 ~39 parasites/barcode, with a Pearson correlation coefficient (PCC) r = 0.9954 within this range (**Fig. 1e**).
134 This confirmed that barcodes could be successfully identified and reliably quantified at relative frequencies
135 as low as 0.0002 (0.02%). Combined these data demonstrated that our pipeline was able to identify
136 individual barcodes within libraries of at least 96-member complexity with high sensitivity.

137

138 ***Barcoded parasite libraries are stably maintained in vitro and in vivo.***

139 To test whether the complexity of the barcode libraries was stably maintained *in vitro* in the absence of host-
140 organism selective pressure, the pooled library of barcoded parasites was serially passaged through human
141 foreskin fibroblasts (HFFs). Lysed-out parasite cultures were sampled every passage (~36 hours) for a period
142 of six passages, equal to a minimum of six complete lytic growth cycles (invasion, replication, egress). The
143 genetic complexity of the barcode population *in vitro* was remarkably stable, with the PCC testing the
144 relationship between barcode abundance at the beginning and end of each 36-hour passage consistently
145 >0.96 (**Fig. 2a, S3a-e)**. This was emphasized by the comparison of the first and last passages (P1 *vs.* P6),
146 which had a PCC of 0.95, demonstrating that the genetic complexity of the 96-member barcode library was
147 stably maintained over multiple rounds of lytic growth (**Fig. S3f**).

148 Following confirmation of *in vitro* stability, we tested our ability to propagate and recover the
149 barcode library *in vivo* within a murine host. For the purposes of this pilot experiment we focused on a 36-
150 hour intra peritoneal infection, reasoning that host immune pressure would be low at this early infection
151 timepoint. Thus the relative stability of the population *in vivo* would be minimally influenced by the host
152 immune system that might complicate interpretation. Four separate inoculums of the complex barcode
153 library pool (0.25×10^6, 0.5×10^6, 1×10^6 or 2×10^6 parasites) were injected intraperitoneally into C57BL/6
154 mice, and the infection allowed to proceed for 36 hours before retrieval of parasites from the peritoneal
155 cavity. For this pilot experiment, the poor growth of a subset of transfected parasites limited the barcode
156 library complexity within the inoculum to 63 strains. Comparison of the infection input with the retrieved
157 output samples showed positive correlation for the highest inoculum, PCC = 0.98 (**Fig. 2b**). This
158 demonstrated that for the highest inoculum and within a 36-hour *in vivo* infection window, the genetic
159 complexity of the barcode library was stable and could be successfully retrieved from the murine host.
160 Combined these data confirmed that, in the absence of significant selective pressures, barcode library
161 complexity was stably maintained *in vitro* and *in vivo*. Reduced correlation observed for the lower dose
162 infections may be attributed to an artificial bottleneck created by inoculum dilution and not to any host-
163 derived process (**Fig. S4a-c)**.

164 Following demonstration that barcoded libraries of parasites could be successfully generated by
165 multiplexed transfection, we tested the limits of our method. We hypothesized that the CRISPR-Cas9
166 strategy used to promote integration of barcode oligos by HDR could support simultaneous integration of
167 multiple individual barcodes across an entire population, within a single transfection. This would simplify
168 complex barcode library production into a single "one-pot" transfection using widely available cuvette-based
169 transfection apparatus. To test this, a single transfection was performed on a single isolated population of
170 parasites using the CRISPR-Cas9 approach described, but with all 96 HDR barcoding oligos combined into a
171 single pool. This pooled transfection was performed in parallel in representative type I and type II parasite
172 strains (RHΔ*ku80* and PruΔ*ku80* respectively), using the same mixed pool of 96 barcode oligo repair
173 templates. FUDR-resistant parasite populations were established, genomic DNA isolated, amplicons
174 prepared, and NGS libraries sequenced. We identified all 96 barcodes within the sequence reads generated
175 from the integration-specific amplicon (**Fig. S5a, b**). Variation between the relative frequencies of individual
176 barcode alleles within the population was observed, indicating the possibility of an unanticipated barcode

177 effect upon parasite fitness. However, comparison of the two independently transfected parasite strains
178 exhibited correlated frequency distributions for the different barcodes (**Fig. 2c, S5c**). We therefore concluded
179 that differences were likely due to the high sensitivity of the readout identifying minor differences in the
180 relative abundance of each barcode HDR template within the pool used for transfection. These data also
181 indicated a higher level of biological reproducibility for one-pot pool transfected libraries than those
182 generated using the original multiplexed transfection approach (**Fig. S2b**). One-pot pool-transfected
183 barcoded populations were used for all subsequent experiments.
184
185 ***Cellular barcodes reveal the population structure of a eukaryotic pathogen infection***
186 The transition of the *T. gondii* infection *in vivo* from the acute to the chronic stage is typified by the spatial
187 redistribution of the parasite into skeletal muscle and the central nervous system (Wohlfert et al., 2017).
188 Colonization of these environments is accompanied by the differentiation of parasites from the tachyzoite
189 lifecycle form into slower growing encysted bradyzoites, which is important for parasite transmission
190 (Barrett et al., 2019). The restrictive nature of the BBB is well documented (Profaci et al., 2020) and we
191 hypothesized that the spatial, temporal, and developmental transitions occurring during the acute-to-chronic
192 infection *in vivo* would impose bottlenecks upon the parasite population represented in the brain. We sought
193 to test this by quantifying changes in the relative frequency distribution of our 96 neutral barcode alleles. An
194 infection study was conceived to assess population structure changes over the course of a full infection,
195 focused on determining the width of the bottleneck experienced by the parasite population as it colonizes the
196 brain of the CBA/J murine host (**Fig. 2d**). We compared changes in the frequency distribution of barcodes in
197 the inoculum, at the acute phase of infection in the peritoneal cavity (at 48 hours) and once chronic infection
198 was established in the brain at day 28. Comparison of independent replicate NGS runs for individual libraries
199 indicated a very high degree of reproducibility (**Fig. S5d**), allowing us to confidently compare samples
200 multiplexed across different NGS runs. Considering the 36-hour pilot infection data using lower inoculums
201 (**Fig. S4**), we anticipated that the dilution of parasite cultures for the inoculum could affect relative
202 frequencies of barcodes within the population and influence our interpretation of data outputs. To control for
203 this, the initial transfected pool was compared to inoculum samples (37,000 tachyzoites) re-expanded *in vitro*
204 (**Fig. 2d**). The artificial bottleneck imposed by dilution led to changes in the relative frequencies of
205 individual barcode, observed through a loss of correlation between the samples (**Fig. S5e**). Although relative

206 frequencies changed, overall library coverage was retained with all 96 barcodes still represented within the
207 population. Independently expanded populations of the same 37,000 parasite inoculum were highly
208 correlated with one another (**Fig. S5f-h**), confirming that *in vitro* expansion of *in vivo* samples would
209 minimally affect library composition. At 48 hours, shifts in the relative frequencies of barcodes within the
210 peritoneal exudate populations were compared to the averaged barcode representation in the inoculum
211 samples (**Fig. 2e, f**), and these changes were unique to each animal. This indicated that stochastic selective
212 pressures likely drive initial selective sweeps during the early stages of the acute infection, and emphasized
213 the need to consider each host organism as a unique environment. After 28 days, brains of chronically
214 infected mice were isolated, and parasites expanded *in vitro.* Unexpectedly, most barcodes were identified in
215 each individual host brain, with extinction events infrequently observed (**Fig. 2g, Table S1**). At the 28-day
216 timepoint the cumulative extinction frequency across all 14 mice was 0.007 (10/1344), with extinction
217 events associated with lower frequency barcodes within the starting infection population (**Table S3)**. We
218 also noted that extinction events were observed in NGS runs with lower total read counts, suggesting that
219 extinctions could be due to reduced sequence sampling depth rather than a true absence of the specific
220 barcoded parasite(s) in the brain (**Table S3**). This indicated that any selection bottleneck experienced by
221 parasites during the colonization of the brain niche must be broad. Taken together these data suggest that
222 with an inoculum of 37,000 parasites (roughly 370 parasites representing each barcode) limited founder
223 effects act on the genetic diversity of the parasite population colonizing the brain.
224
225 ***The brain niche is permissive to colonization by T. gondii***
226 To better understand the process of colonization, we sought to quantify the effective population size in the
227 brain and estimate the width of the acute-to-chronic infection bottleneck. Sequence tag-based analysis of
228 microbial populations (STAMP) (Abel et al., 2015) frames molecular barcodes as neutral alleles, enabling
229 classical population genetic theory and equations for effective population size estimates (N_e) (Charlesworth,
230 2009) to be applied to NGS datasets. The relative frequencies of all barcodes in a complex population are
231 converted into a single metric of population diversity, which provides a direct estimation of founder
232 population size, and approximates bottleneck width ($N_e \approx N_b$). Due to fundamental differences in virulence of
233 *Toxoplasma* strains (Behnke et al., 2011, Reikvam and Lorentzen-Styr, 1976), we anticipated that the
234 absolute founder number would be strongly influenced by the genetic background of both the parasite and

235 the host (Watson and Davis, 2019). In light of this we sought to quantify relative changes in N_b as an
236 indication of populations having been through a genetic selection bottleneck, analysing our dataset with the
237 equations defined in the STAMP methodology (Abel et al., 2015). Our initial analyses indicated that
238 compared to the infection inoculum, the population within the brain had experienced a restrictive bottleneck
239 resulting in an ~100-fold reduction in N_b (**Fig. 2h**). Future experiments including further calibration of N_b are
240 necessary before any conclusive statement regarding the absolute founder population number can be
241 accurately made (Abel et al., 2015). Despite this, the consistency in the calculated N_b between the different
242 individual host animals was remarkable. To further assess how N_b changed over the course of the infection
243 we performed the same analysis of read data obtained from parasites populations within the peritoneal cavity
244 after 48 hours, retrieved as the acute infection is being established. Surprisingly, the change in N_b at this
245 early acute phase of the infection relative to the inoculum was similar that seen at 28 days (**Fig. 2h**). For one
246 infection, the change in N_b was intermediate to that observed for the other mice in the group. Due to the
247 terminal nature of parasite retrieval from the host, it was not possible to directly compare the relative
248 frequency distribution of barcodes for a single inoculum replicate at the two points of infection in a single
249 animal. However, on the basis of these data we hypothesize that the most restrictive bottleneck experienced
250 by *T. gondii* during the course of an infection is within the early acute phase, with the BBB imposing
251 negligible further restriction upon the parasite population diversity during colonization of the brain niche.
252 This interpretation of the relative N_b values for the different stages of the infection is consistent with the
253 detection of most barcoded parasite strains within the brains of chronically infected mice (**Fig. 2g**).
254 Calculation of genetic distance (chord distance) is an additional way to quantify the genetic similarity of
255 complex populations derived from one another, such as those obtained from different tissues and phases of
256 infection (Abel et al., 2015, Cavalli-Sforza and Edwards, 1967). Bottlenecks lead to substantial genetic drift
257 between populations, with greater chord distances indicative of a loss of population "relatedness". Applying
258 these equations, we found that there was no significant difference in chord distances between the populations
259 at the different stages of infection relative to the starting population (**Fig. 2i**). These data indicate that there is
260 no further genetic drift experienced by the parasite population following the initial acute phase as the brain is
261 colonized. This further supports our data suggesting an absence of restrictive genetic selection bottlenecks
262 during the establishment of the chronic phase of the *T. gondii* infection.
263

264 **Discussion**

265 A key role of the BBB is to restrict pathogen access to the immune-privileged brain niche (Kim, 2008).
266 Unexpectedly our findings imply multiple, unique colonization events occur in the brain during chronic
267 infection. Neuronal tissue is rich in fats, and in the case of prey species such as mice, represents a high-
268 energy nutritional food component in the diets of predator species such as felids (Plantinga et al., 2011).
269 Feline consumption of high-energy infected neuronal tissue of prey provides *T. gondii* with a route back into
270 the definitive feline host (Dubey, 1997), and is an evolutionary strategy which increases the likelihood of
271 feline transmission. A means to evade any restrictive bottleneck when colonizing the brain niche would be
272 consistent with this evolutionary strategy, supporting maximal transmission of genetic diversity into the
273 feline host to contribute to recombination in the subsequent sexual cycle. From the evolutionary perspective
274 of the parasite this would be highly advantageous. The synergistic alignment of this macro scale ancient
275 predator-prey relationship with the molecular features of the *T. gondii* host-pathogen interaction is truly
276 remarkable.

277 The discoveries made in this study would have not been possible without a means to barcode this
278 eukaryotic pathogen. Molecular barcoding has provided critical insights into the infection biology of viruses
279 such as poliovirus (Kuss et al., 2008, Pfeiffer and Kirkegaard, 2006), and bacteria such as *Salmonella* (Grant
280 et al., 2008, Lam and Monack, 2014, Lim et al., 2014, Kaiser et al., 2013), and we anticipate that barcoded
281 *Toxoplasma* strains will have similar far reaching application. While barcode sequencing strategies have
282 been leveraged for eukaryotic pathogen phenotypic screens (Alsford et al., 2011, Bushell et al., 2017, Sidik
283 et al., 2016), to our knowledge this is the first use of cellular barcodes to study the within-host infectious
284 population structure of a eukaryotic pathogen. Our simple oligo barcoding strategy can be applied to any
285 system accessible to CRISPR that contains endogenous or engineered negative selection markers. Our
286 approach allows for parallel integration of even greater numbers of unique barcodes which, combined with
287 STAMP (Abel et al., 2015), will provide increased precision in future host-pathogen population genetic
288 studies and quantification of the absolute founder population number. With particular application to this
289 complex host-pathogen interaction, researchers can now probe the within-host population genetics of the
290 infection with an unprecedented degree of molecular resolution.

291

292

293 **Methods**

294 **Parasite cell culture:** T. gondii parasite strains were maintained by serial passage in confluent human
295 foreskin fibroblasts (HFF-1 ATCC® SCRC-1041™). HFFs were cultured at 37 °C with 5% CO2 in
296 Dulbecco's Modified Eagle's medium supplemented with 10% foetal bovine serum and 2 mM L-glutamine.
297 Tachyzoites were harvested via mechanical syringe lysis of heavily infected HFFs through a 25-gauge
298 needle. RHΔ*ku80* parasites were used for *in vivo* and *in vitro* studies. PruΔ*ku80* parasites were used in in
299 vivo experiments where chronic infections were established. Parasite strains were received as a kind gift
300 from Dr Moritz Treeck.

301

302 **Generation of barcoded *T. gondii* strains and libraries:** 60-nucleotide single strand oligos were designed
303 to include a unique 6 nucleotide barcode sequence flanked by a stop codon and homology regions on either
304 side. The sequences of all oligos within the 96-member library can be found in **Table S2.** Barcoded libraries
305 of tachyzoites were generated using two alternative strategies: For strategy A, 96 independent transfections
306 were carried out in 16 well Nucleocuvette strips. 10 µg of the pSAG1::Cas9-U6::sgUPRT vector (Shen et al.,
307 2014) and 10 µg of the barcode oligo (equivalent to an ~1:160 molar ratio of plasmid to oligo) were co-
308 transfected into approximately 1×10^6 extracellular tachyzoites using the 4D-Nucleofector X Unit programme
309 F1-115 (Lonza). 24 hours post-transfection, transgenic barcoded parasites were selected for using 5 µM 5'-
310 fluro-2'-deoxyuridine (FUDR). Barcoded strains were independently maintained, and only pooled just prior
311 to use. For strategy B, a single "one-pot" transfection was carried out. An oligo library pool containing
312 roughly equal amounts of all barcode oligos was prepared. The ratio of the pSAG1::Cas9-U6::sgUPRT
313 vector to oligo pool was the same as in strategy A, though here the final concentration of any single oligo
314 within the pool will be ~100-fold less. Transfection and selection was performed as for A, with the complex
315 barcoded strain library generated and maintained as a single population.

316

317 **NGS library preparation:** Frozen cell pellets of extracellular tachyzoites were thawed to room temperature
318 and genomic DNA extracted using the DNeasy Blood & Tissue Kit (Qiagen). Genomic DNA libraries were
319 prepared following the 16S Metagenomic Sequencing Library Preparation guide (Illumina). In brief, an ~300
320 base pair amplicon region containing the 6 nt barcode sequence was amplified from the barcoded UPRT
321 locus using primer sequences (5′ to 3′)

322 **TCGTCGGCAGCGTCAGATGTGTATAAGAGACAG**tggatgtgtcataccatggagtttcctg and
323 **GTCTCGTGGGCTCGGAGATGTGTATAAGAGACAG**tgttttagtgtaacaaagtggacagcagc. These primer
324 sequences include the specified Illumina adapter overhang sequences (bold, uppercase). AMPure XP beads
325 were used to purify the resulting PCR product. An indexing PCR was carried using the purified product as
326 the template to ligate dual indices and sequencing adapters to the amplicon using the Nextera XT Index Kit
327 (Illumina). Indexed libraries were then cleaned using AMPure XP beads and quantified on the Quantus
328 Fluorometer using the QuantiFluor ONE dsDNA System (Promega). Amplicons were purity-checked and
329 sized on a TapeStation using D1000 ScreenTape System (Agilent). For each NGS run, typically 8 to 25
330 uniquely indexed libraries were pooled at equimolar concentrations for multiplexed outputs on either an
331 Illumina MiSeq or NextSeq sequencer using the MiSeqV3 PE 75 bp kit or NextSeq 500/550 Mid Output
332 v2.5 PE 75 bp kit respectively. PhiX DNA spike-in of 20% was used in all NGS. Following acquisition,
333 sequencing data was demultiplexed and total sample reads extracted from fastq files using the Galaxy web
334 platform. Sequencing reads were then concatenated, trimmed, and split into the respective barcodes. Phred
335 QC scores for all NGS runs were >30 with the exception of a single run used for analysis of technical and
336 biological replicates, which still gave an acceptable score of 28. Following trimming to the appropriate 6 nt
337 region a stringent barcode mismatch tolerance of 0% was applied, typically resulting in 10-15% of total
338 reads being discarded. Barcode read data was analysed using Prism 8 and correlations coefficients calculated
339 within the software using Pearson analysis.
340
341 **Mice:** 6-week old female C57BL/6 or CBA/J mice were purchased from Jackson Laboratories. Mice were
342 acclimated for 7 days prior to infection. For studies using CBA/J mice, the animal protocols were approved
343 by the University of Virginia Institutional Animal Care and Use Committee (protocol # 4107-12-18). All
344 animals were housed and treated in accordance with AAALAC and IACUC guidelines at the University of
345 Virginia Veterinary Service Center. The procedures involving C57BL/6 mice were approved by the local
346 ethical committee of the Francis Crick Institute Ltd, Mill Hill Laboratory and are part of a project license
347 approved by the Home Office, UK, under the Animals (Scientific Procedures) Act 1986.
348
349 **Mouse infections:** The pooled barcode parasite library was expanded on HFFs in a T175 flask. Once full
350 parasite vacuoles were observed, parasites were scraped and syringe lysed, counted on a haemocytometer

351 and diluted to an inoculum of 37,000 viable parasites in 200 µL of PBC per mouse. The viability of parasites
352 in the inoculum was confirmed by plaque assay. At the time of inoculation 2×10^6 parasites were frozen as an
353 initial population control. In addition, three inoculum control samples were expanded immediately on HFF
354 T25 flasks. After 48 hours three mice were euthanized to isolate parasites in the peritoneal exudate.
355 Specifically, 10 mL of PBS was injected by 25G needle into the peritoneal cavity, mice were rocked
356 vigorously and peritoneal fluid removed by syringe. Parasites and exudate cells were washed twice in 10 mL
357 of media containing penicillin/streptomycin, pelleted at 1,500 rpm and plated on HFFs T25 flasks. Parasites
358 were harvested when they approached full lysis of the monolayer pelleted and frozen for genomic DNA
359 isolation. After 28 days the remaining mice were euthanized. Carcasses were incubated in 20% bleach for 10
360 minutes and the brain was excised in the biosafety cabinet under sterile conditions. To isolate parasites the
361 brains were mashed though a 70 µm filter using 25mL PBS with 5% FBS and penicillin/streptomycin. Brain
362 mash was pelleted for 10 minutes at 1,500 rpm, washed twice then plated on HFF monolayers in T75 flasks.
363 After 36 hours, media was changed to remove debris. Parasites were harvested by syringe lysis when the
364 HFF monolayer was nearly lysed out (approximately 2 weeks), pelleted and frozen for genomic DNA
365 isolation. To validate cyst formation in the brain at 28 days post infection 1/50th of the mash was reserved,
366 fixed in 4% paraformaldehyde for 15 minutes then stained with a 1:500 dilution of dolichos bifluorus
367 agglutinin conjugated to FITC in PBS (Vector Labs). FITC-positive cysts were confirmed under 20x
368 magnification.
369
370 **Bottleneck Analysis and Chord Distance Calculations:** Genetic selection bottlenecks experienced within
371 the murine host were estimated by calculating changes in the relative frequencies of barcodes within
372 dynamic T. gondii populations in relation to the starting population in the inoculum. Calculations of
373 bottleneck width (N_b) were performed according to method outlined by Abel *et al* (Abel et al., 2015) using
374 the following equations:
375
376 $$\hat{F} = \frac{1}{k}\sum_{i=1}^{k}\frac{(f_{i,s} - f_{i,0})^2}{f_{i,0}(100 - f_{i,0})}$$
377
378 $$N_b \approx N_e = \frac{g}{\hat{F} - \frac{1}{S_0} - \frac{1}{S_s}}$$

k = number of distinct alleles
$f_{i,0}$ = frequency of allele i at time 0
$f_{i,s}$ = frequency of allele i at sampling
g = number of generations during competitive growth
S_0 = sample size at time 0
S_s = sample size at sampling

379

380 The following equations (Cavalli-Sforza and Edwards, 1967) were used to calculate chord distance:

381

382 $$D_{ch} = \frac{2\sqrt{2}}{\pi}\sqrt{1-\cos\theta}$$

383

384 $$\cos\theta = \sum_{i=1}^{k}\sqrt{f_{P1,i}f_{P2,i}}$$

385

D_{ch} = chord distance
k = number of distinct alleles
$f_{P1,i}$ = frequency of allele i in population 1
$f_{P2,i}$ = frequency of allele i in population 2

386

387 **References**

388 ABEL, S., ABEL ZUR WIESCH, P., CHANG, H. H., DAVIS, B. M., LIPSITCH, M. & WALDOR, M. K.
389 2015. Sequence tag-based analysis of microbial population dynamics. *Nat Methods,* 12**,** 223-6, 3 p
390 following 226.

391 AFGAN, E., BAKER, D., BATUT, B., VAN DEN BEEK, M., BOUVIER, D., CECH, M., CHILTON, J.,
392 CLEMENTS, D., CORAOR, N., GRUNING, B. A., GUERLER, A., HILLMAN-JACKSON, J.,
393 HILTEMANN, S., JALILI, V., RASCHE, H., SORANZO, N., GOECKS, J., TAYLOR, J.,
394 NEKRUTENKO, A. & BLANKENBERG, D. 2018. The Galaxy platform for accessible,
395 reproducible and collaborative biomedical analyses: 2018 update. *Nucleic Acids Res,* 46**,** W537-
396 W544.

397 ALSFORD, S., TURNER, D. J., OBADO, S. O., SANCHEZ-FLORES, A., GLOVER, L., BERRIMAN, M.,
398 HERTZ-FOWLER, C. & HORN, D. 2011. High-throughput phenotyping using parallel sequencing
399 of RNA interference targets in the African trypanosome. *Genome Res,* 21**,** 915-24.

400 BARRETT, M. P., KYLE, D. E., SIBLEY, L. D., RADKE, J. B. & TARLETON, R. L. 2019. Protozoan
401 persister-like cells and drug treatment failure. *Nat Rev Microbiol,* 17**,** 607-620.

402 BEHNKE, M. S., KHAN, A., WOOTTON, J. C., DUBEY, J. P., TANG, K. & SIBLEY, L. D. 2011.
403 Virulence differences in Toxoplasma mediated by amplification of a family of polymorphic
404 pseudokinases. *Proc Natl Acad Sci U S A,* 108**,** 9631-6.

405 BLUNDELL, J. R. & LEVY, S. F. 2014. Beyond genome sequencing: lineage tracking with barcodes to
406 study the dynamics of evolution, infection, and cancer. *Genomics,* 104**,** 417-30.

407 BUSHELL, E., GOMES, A. R., SANDERSON, T., ANAR, B., GIRLING, G., HERD, C., METCALF, T.,
408 MODRZYNSKA, K., SCHWACH, F., MARTIN, R. E., MATHER, M. W., MCFADDEN, G. I.,

409 PARTS, L., RUTLEDGE, G. G., VAIDYA, A. B., WENGELNIK, K., RAYNER, J. C. &
410 BILLKER, O. 2017. Functional Profiling of a Plasmodium Genome Reveals an Abundance of
411 Essential Genes. *Cell,* 170**,** 260-272 e8.
412 CAVALLI-SFORZA, L. L. & EDWARDS, A. W. 1967. Phylogenetic analysis. Models and estimation
413 procedures. *Am J Hum Genet,* 19**,** 233-57.
414 CHARLESWORTH, B. 2009. Fundamental concepts in genetics: effective population size and patterns of
415 molecular evolution and variation. *Nat Rev Genet,* 10**,** 195-205.
416 DONALD, R. G. & ROOS, D. S. 1995. Insertional mutagenesis and marker rescue in a protozoan parasite:
417 cloning of the uracil phosphoribosyltransferase locus from Toxoplasma gondii. *Proc Natl Acad Sci*
418 *U S A,* 92**,** 5749-53.
419 DUBEY, J. P. 1997. Tissue cyst tropism in Toxoplasma gondii: a comparison of tissue cyst formation in
420 organs of cats, and rodents fed oocysts. *Parasitology,* 115 (Pt 1)**,** 15-20.
421 ELSHEIKHA, H. M. & KHAN, N. A. 2010. Protozoa traversal of the blood-brain barrier to invade the
422 central nervous system. *FEMS Microbiol Rev,* 34**,** 532-53.
423 GRANT, A. J., RESTIF, O., MCKINLEY, T. J., SHEPPARD, M., MASKELL, D. J. & MASTROENI, P.
424 2008. Modelling within-host spatiotemporal dynamics of invasive bacterial disease. *PLoS Biol,* 6**,**
425 e74.
426 HUYNH, M. H. & CARRUTHERS, V. B. 2009. Tagging of endogenous genes in a Toxoplasma gondii
427 strain lacking Ku80. *Eukaryot Cell,* 8**,** 530-9.
428 KAISER, P., SLACK, E., GRANT, A. J., HARDT, W. D. & REGOES, R. R. 2013. Lymph node
429 colonization dynamics after oral Salmonella Typhimurium infection in mice. *PLoS Pathog,* 9**,**
430 e1003532.
431 KEBSCHULL, J. M. & ZADOR, A. M. 2018. Cellular barcoding: lineage tracing, screening and beyond.
432 *Nat Methods,* 15**,** 871-879.
433 KIM, K. S. 2008. Mechanisms of microbial traversal of the blood-brain barrier. *Nat Rev Microbiol,* 6**,** 625-
434 34.
435 KUSS, S. K., ETHEREDGE, C. A. & PFEIFFER, J. K. 2008. Multiple host barriers restrict poliovirus
436 trafficking in mice. *PLoS Pathog,* 4**,** e1000082.

437 LAM, L. H. & MONACK, D. M. 2014. Intraspecies competition for niches in the distal gut dictate
438 transmission during persistent Salmonella infection. *PLoS Pathog,* 10**,** e1004527.
439 LIM, C. H., VOEDISCH, S., WAHL, B., ROUF, S. F., GEFFERS, R., RHEN, M. & PABST, O. 2014.
440 Independent bottlenecks characterize colonization of systemic compartments and gut lymphoid
441 tissue by salmonella. *PLoS Pathog,* 10**,** e1004270.
442 LUFT, B. J., HAFNER, R., KORZUN, A. H., LEPORT, C., ANTONISKIS, D., BOSLER, E. M.,
443 BOURLAND, D. D., 3RD, UTTAMCHANDANI, R., FUHRER, J., JACOBSON, J. & ET AL.
444 1993. Toxoplasmic encephalitis in patients with the acquired immunodeficiency syndrome.
445 Members of the ACTG 077p/ANRS 009 Study Team. *N Engl J Med,* 329**,** 995-1000.
446 PFEIFFER, J. K. & KIRKEGAARD, K. 2006. Bottleneck-mediated quasispecies restriction during spread of
447 an RNA virus from inoculation site to brain. *Proc Natl Acad Sci U S A,* 103**,** 5520-5.
448 PLANTINGA, E. A., BOSCH, G. & HENDRIKS, W. H. 2011. Estimation of the dietary nutrient profile of
449 free-roaming feral cats: possible implications for nutrition of domestic cats. *Br J Nutr,* 106 Suppl 1**,**
450 S35-48.
451 PROFACI, C. P., MUNJI, R. N., PULIDO, R. S. & DANEMAN, R. 2020. The blood-brain barrier in health
452 and disease: Important unanswered questions. *J Exp Med,* 217.
453 REIKVAM, A. & LORENTZEN-STYR, A. M. 1976. Virulence of different strains of Toxoplasma gondii
454 and host response in mice. *Nature,* 261**,** 508-9.
455 RIBET, D. & COSSART, P. 2015. How bacterial pathogens colonize their hosts and invade deeper tissues.
456 *Microbes Infect,* 17**,** 173-83.
457 SHEN, B., BROWN, K. M., LEE, T. D. & SIBLEY, L. D. 2014. Efficient gene disruption in diverse strains
458 of Toxoplasma gondii using CRISPR/CAS9. *mBio,* 5**,** e01114-14.
459 SIDIK, S. M., HUET, D., GANESAN, S. M., HUYNH, M. H., WANG, T., NASAMU, A. S., THIRU, P.,
460 SAEIJ, J. P., CARRUTHERS, V. B., NILES, J. C. & LOURIDO, S. 2016. A Genome-wide CRISPR
461 Screen in Toxoplasma Identifies Essential Apicomplexan Genes. *Cell,* 166**,** 1423-1435 e12.
462 SMITH, A. M., HEISLER, L. E., MELLOR, J., KAPER, F., THOMPSON, M. J., CHEE, M., ROTH, F. P.,
463 GIAEVER, G. & NISLOW, C. 2009. Quantitative phenotyping via deep barcode sequencing.
464 *Genome Res,* 19**,** 1836-42.

465 WALDMAN, B. S., SCHWARZ, D., WADSWORTH, M. H., 2ND, SAEIJ, J. P., SHALEK, A. K. &
466 LOURIDO, S. 2020. Identification of a Master Regulator of Differentiation in Toxoplasma. *Cell,*
467 180**,** 359-372 e16.
468 WATSON, G. F. & DAVIS, P. H. 2019. Systematic review and meta-analysis of variation in Toxoplasma
469 gondii cyst burden in the murine model. *Exp Parasitol,* 196**,** 55-62.
470 WOHLFERT, E. A., BLADER, I. J. & WILSON, E. H. 2017. Brains and Brawn: Toxoplasma Infections of
471 the Central Nervous System and Skeletal Muscle. *Trends Parasitol,* 33**,** 519-531.
472

473 **Acknowledgements:**
474 This work was supported by grants NC/S001239/1 from the NC3Rs (to C.J.W and M.A.C), and
475 202553/Z/16/Z from the Wellcome Trust & Royal Society (to M.A.C.). This work was also supported by
476 the Francis Crick Institute (FC001076 to EMF), which receives its core funding from Cancer
477 Research UK, the UK Medical Research Council, and the Wellcome Trust. EMF was supported by
478 a Senior Wellcome Trust Fellowship (217202/Z/19/Z). The Imperial BRC Genomics Facility provided
479 resources and support that contributed to the research results reported within this paper. The Imperial BRC
480 Genomics Facility is supported by NIHR funding to the Imperial Biomedical Research Centre. Ivan Andrew,
481 JP Haywood and Laurence Game at the UKRI London Institute of Medical Sciences Genomics Laboratory.
482 We would also like to thank Dr Ellen M. McDonagh for critical reading of the manuscript.
483

484 **Author Contributions:** Conception/design of the work: EF, SEE, MAC. Acquisition/analysis/interpretation
485 of data: CJW, GS, MB, EDSA, HJB, SEE, MAC. Manuscript drafting and revision: CJW, GS, EDSA, HJB,
486 EF, SEE, MAC
487

488 **Competing interests:** The authors declare no competing interests.
489

490 **Materials & Correspondence**: All correspondence and material requests should be addressed to MAC,
491 m.child@imperial.ac.uk
492

493 **Figure 1**

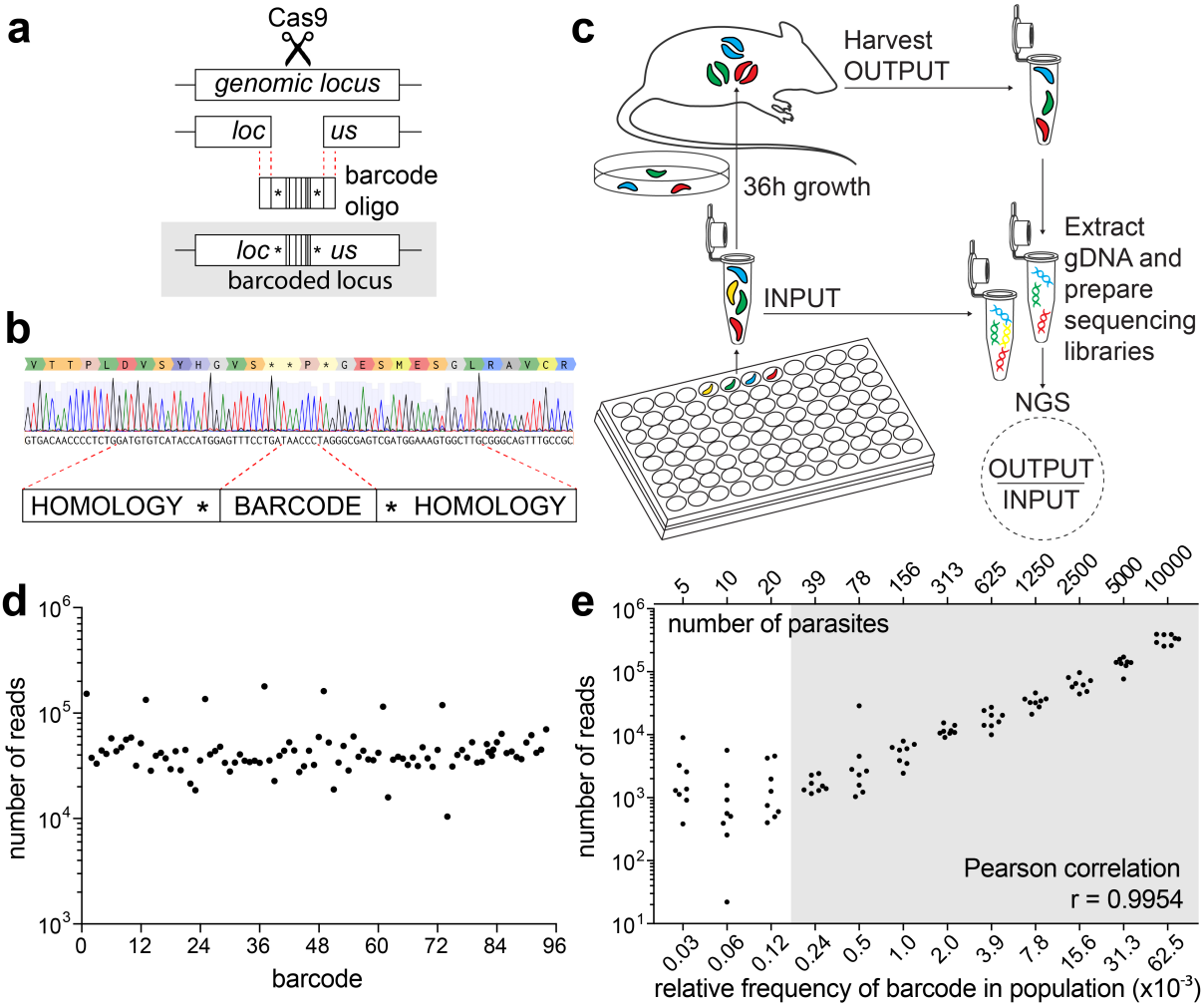

494

495 **Figure 1: *T. gondii* tachyzoites can be molecularly barcoded using a simple CRISPR-based strategy. a)**
496 Schematic of molecular barcoding strategy. A CRISPR guide RNA targets Cas9 to the *UPRT* locus, where
497 Cas9 endonuclease activity introduces a double strand break. This break is repaired by HDR, with the co-
498 transfected 60mer barcode oligo used as the donor template. **b**) Sanger sequencing confirmation that barcode
499 integration results in the simultaneous disruption of the *UPRT* coding sequence, destruction of the
500 protospacer DNA sequence and PAM. **c**) Multiplexed transfection strategy and NGS pipeline to generate
501 barcoded libraries of *T. gondii* tachyzoites for *in vitro* and *in vivo* studies. **d**) Complex libraries containing 96
502 uniquely barcoded strains can be produced, with individual barcodes identified and quantified within NGS
503 datasets. Scatter plot presents read counts for individual barcodes. **e**) Individual barcodes can be detected at
504 low frequencies, and read depth is a sensitive proxy for parasite number. Scatter plot presents number of
505 reads for a serial two-fold dilution series of known numbers of parasites and the relative frequency of

individual barcodes in the population. The shaded area indicates the data used to calculate the PCC provided: $r = 0.9954$, $n = 9$, P (two-tailed) = <0.0001.

535 **Figure 2**

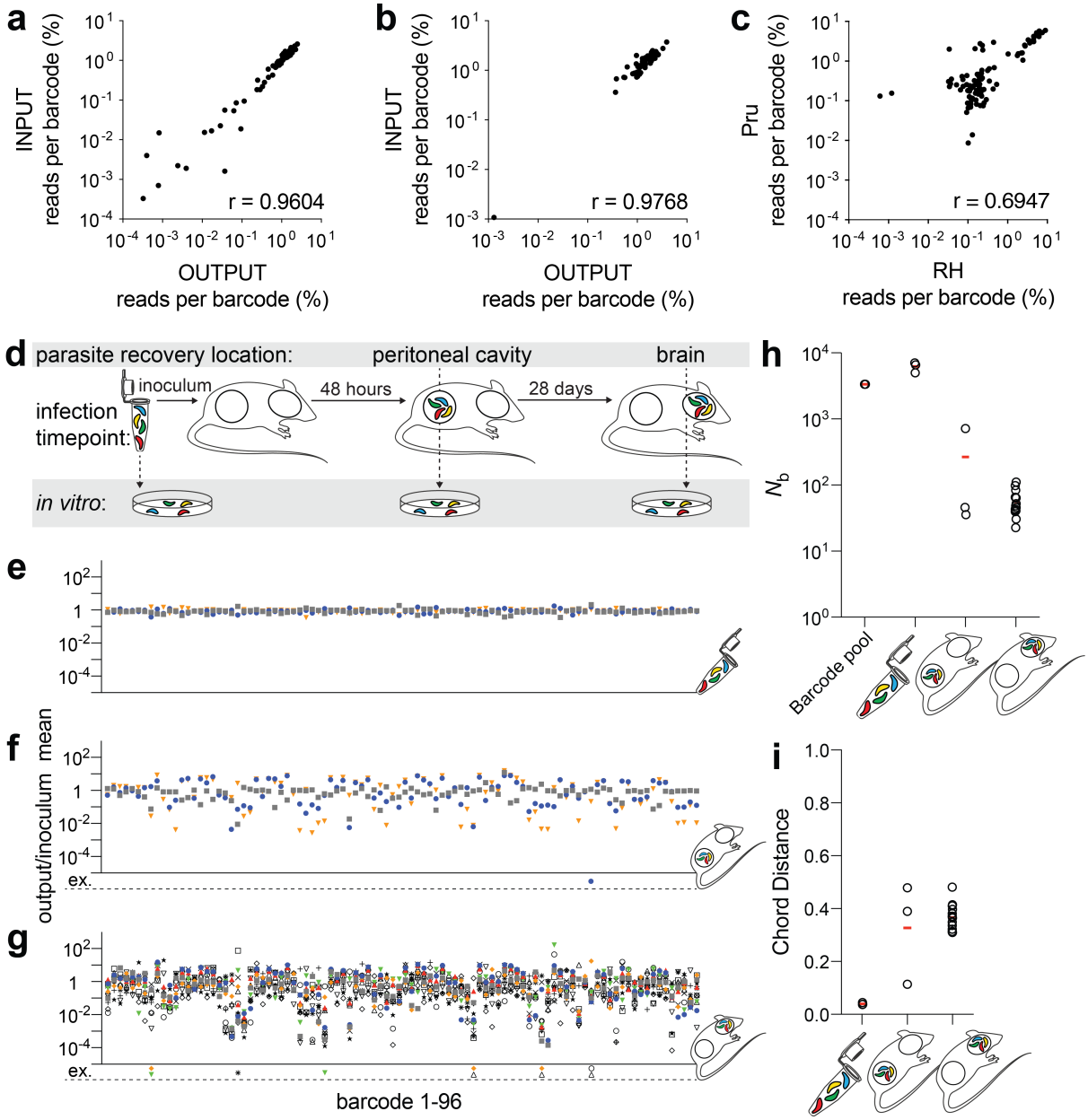

536

537

538 **Figure 2: Barcoded libraries of *T. gondii* parasites are stably maintained *in vitro* and *in vivo*, and can**
539 **be generated via one-pot transfections. a)** The population structure of complex barcode libraries is stable
540 *in vitro*. Scatter plot comparing individual barcode frequencies within the complex pooled library population
541 for an INPUT sample (used for the *in vitro* infection) and the OUTPUT sample harvested following a single
542 lytic growth cycle (~36 hours). PCC r = 0.96, n = 96, P (two-tailed) = <0.0001. **b**) The population structure
543 of complex barcode libraries is stable during early stages of an *in vivo* infection. Scatter plot comparing
544 individual barcode frequencies within a pooled library population for an INPUT sample (the peritoneal
545 infection inoculum) and the OUTPUT sample harvested from the peritoneal cavity following 36 hours of

growth. PCC r = 0.98, n = 63, P (two-tailed) = <0.0001. **c**) Scatter plot of relative barcode frequencies comparing barcoded libraries of parasites generated for two different *T. gondii* strains (RHΔ*ku80* and PruΔ*ku80*) where the one-pot transfection was performed using the same pool of barcoding oligos. PCC r = 0.69, n = 96, P (two-tailed) = <0.0001. PCC values provided on scatter plots indicate degree of correlation between different populations being compared. **d)** Schematic of an experiment investigating changes in the population structure of *T. gondii* over the course of a 28-day *in vivo* infection. The infection is artificially initiated within the peritoneal cavity (, and the infectious population structure monitored at an early acute (48 hours) and chronic phase (28 days). The timepoints are compared to the inoculum mean to identify host bottlenecks restricting diversity. **e-g**) Scatter plot of changes in individual barcode frequencies relative to the inoculum mean in the inoculum (**e**), the peritoneal cavity at 48 hours, n = 3 (**f**), and the brain at 28 days, n = 14 (**g**). Barcode extinctions (ex.) are indicated below the x-axis in the corresponding position to the absent barcoded strain (see also table S1). **h**) Scatter plot of calculated N_b values for parasite populations presents relative changes in total population barcode frequencies during the establishment of the acute and chronic infection in the peritoneal cavity and brain respectively. **i**) Scatter plot of calculated chord distances presents the relatedness and genetic distance between two distinct population samples (acute and chronic) relative to the starting population in the inoculum.

575 **Supplemental Material**

576

577 **Table S1**

Infection timepoint:	48 hours			28 days													
Mouse #	1	2	3	1	2	3	4	5	6	7	8	9	10	11	12	13	14
Barcode #	-	79	-	-	-	8, 60, 71	-	8, 36	-	-	79	-	60, 71, 79	-	-	-	22
Total read #	$14x10^6$	$0.59x10^6$	$2.3x10^6$	$8.3x10^6$	$10x10^6$	$0.62x10^6$	$6.3x10^6$	$0.46x10^6$	$8.0x10^6$	$3.3x10^6$	$1.8x10^6$	$4.1x10^6$	$0.73x10^6$	$5.0x10^6$	$1.7x10^6$	$4.2x10^6$	$0.92x10^6$

578

579 **Table S1:** Details of barcode extinctions occurring during the different phases of infection. Barcode numbers
580 and the mouse in which the extinction was observed are noted. Extinctions are defined by an absence of the
581 barcode sequence within the processed NGS read data.

582

583

584 **Figure S1**

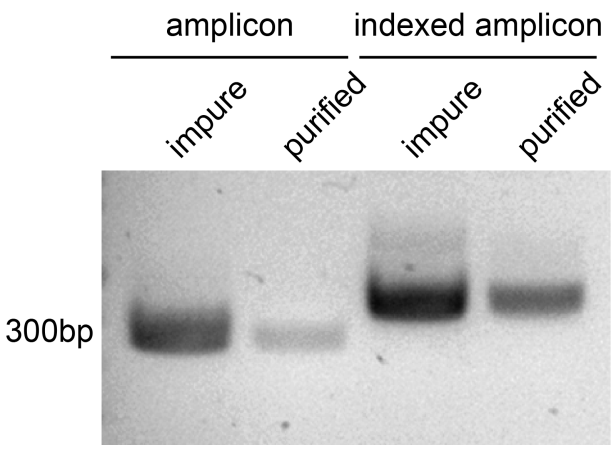

585

586

587 **Figure S1: Construction of NGS libraries for amplicon deep sequencing.** A single ~300 bp amplicon was
588 amplified from genomic DNA, and purified (amplicon, lanes 1 and 2). The purified amplicon was then
589 indexed and re-purified prior to quantification and sizing (indexed amplicon, lanes 3 and 4).

590

591

592

593

594

595 **Figure S2**

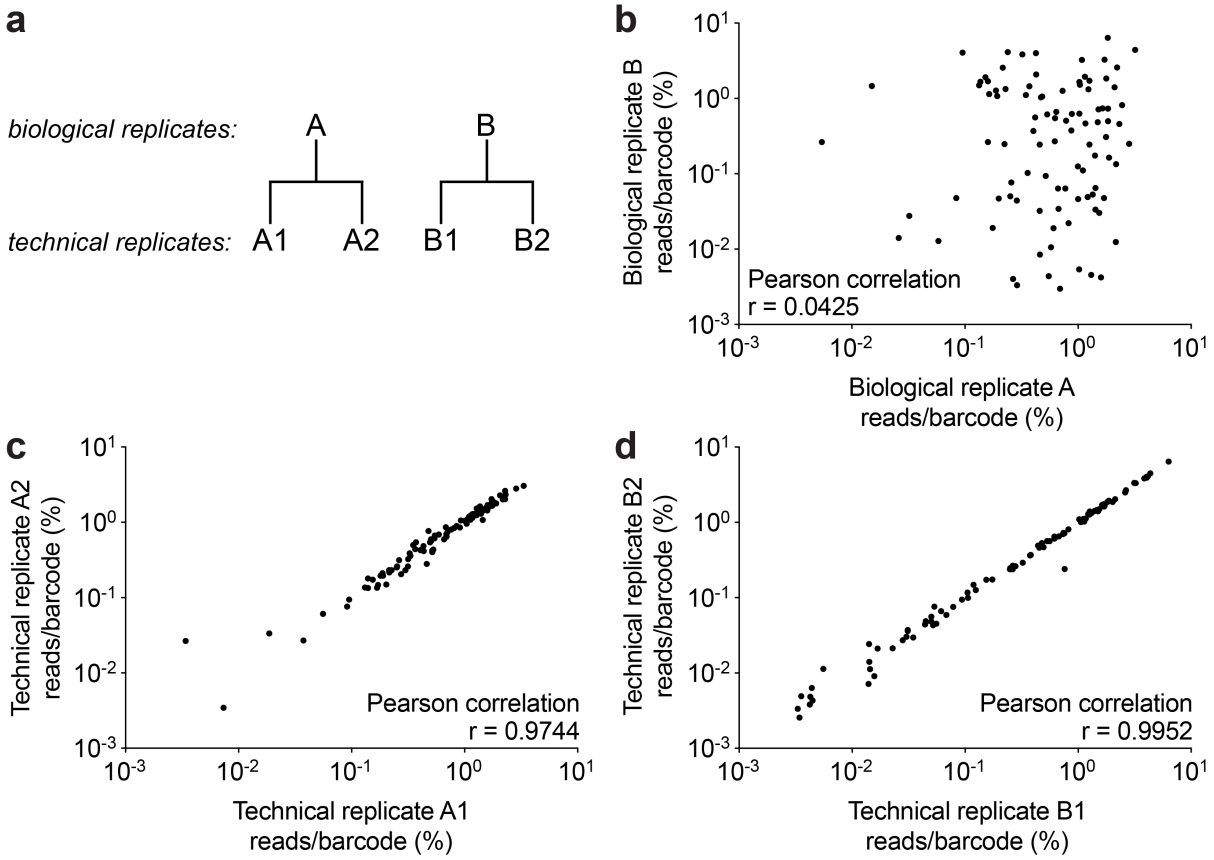

596

597

598 **Figure S2: Analysis of experimental variation for barcoded parasite libraries and NGS pipeline. a)**
599 Strategy to identify the primary major source of variation within the multiplexed transfection barcoding
600 strategy and NGS pipeline. Scatter plots present data comparing the percentage representation of individual
601 barcodes within library pools for (**b**) biological replicates, PCC r = 0.0425, n = 96, P (two-tailed) = 0.6807
602 (n.s.), and technical replicates (**c**) PCC r = 0.9744, n = 96, P (two-tailed) = <0.0001 , and (**d**) PCC r =
603 0.9952, n = 96, P (two-tailed) = <0.0001. PCC values provided on scatter plots indicate degree of correlation
604 between different populations being compared.

605

606

607

608

609

610

611

612 **Figure S3**

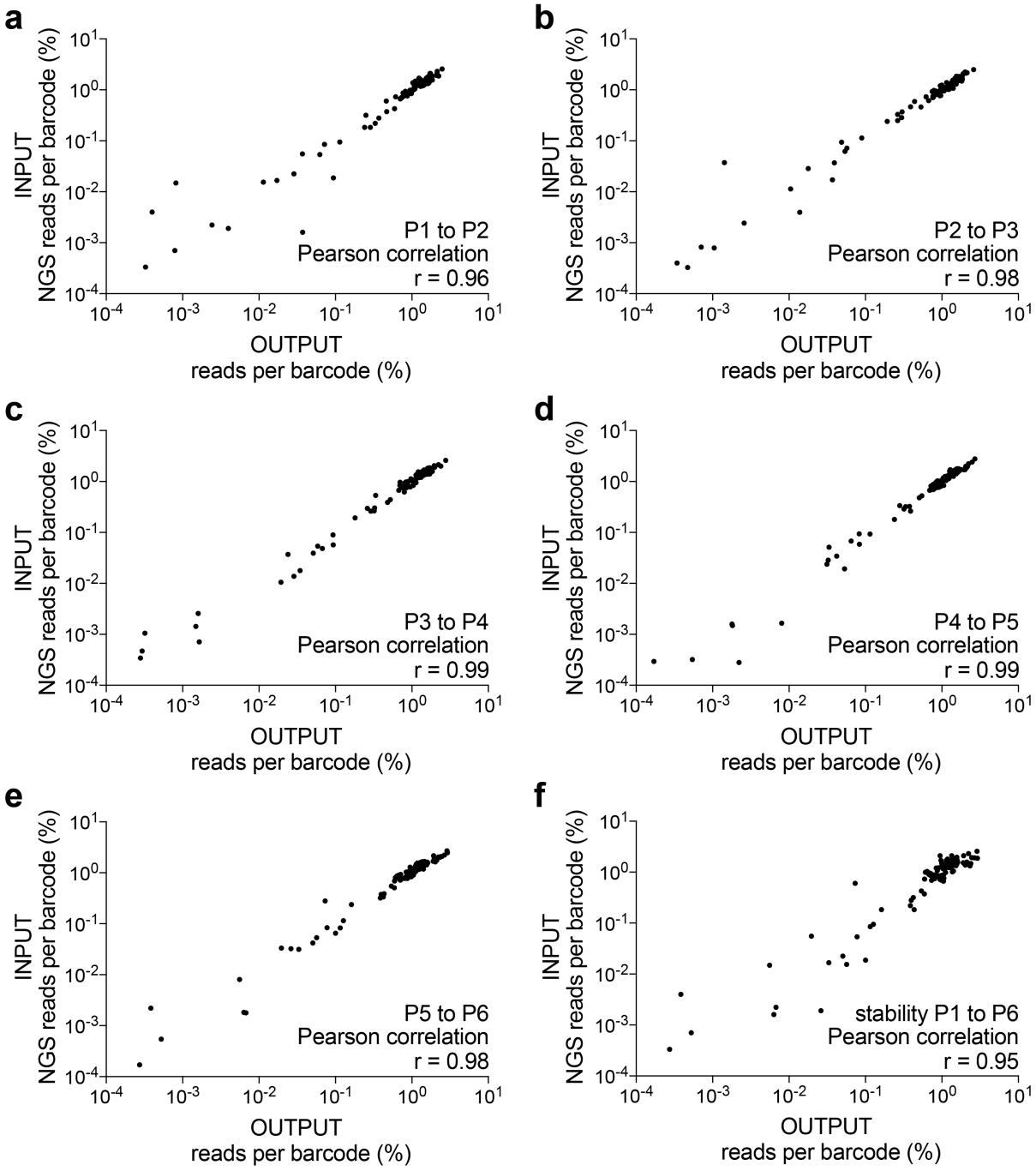

613

614

615 **Figure S3: Assessment of barcoded strain library *in vitro* stability.** A barcoded library of parasites was
616 serially passaged through HFF host cells, and sampled following the completion of each lytic cycle (~36
617 hours/passage). Scatter plots present data comparing the percentage representation of individual barcodes
618 within library pools for the passages indicated on the plots. (**a**) is a repeat of data presented in figure 2a, and
619 shown here for completeness and comparison alongside the entire serial passage experiment dataset. PCC
620 values provided on scatter plots indicate degree of correlation between different populations being

compared: PCC **a**) r = 0.96, n = 96, P (two-tailed) = <0.0001. **b**) r = 0.98, n = 96, P (two-tailed) = <0.0001. **c**) r = 0.99, n = 96, P (two-tailed) = <0.0001. **d**) r = 0.99, n = 96, P (two-tailed) = <0.0001. **e**) r = 0.98, n = 96, P (two-tailed) = <0.0001. **f**) r = 0.95, n = 96, P (two-tailed) = <0.0001.

650 **Figure S4**

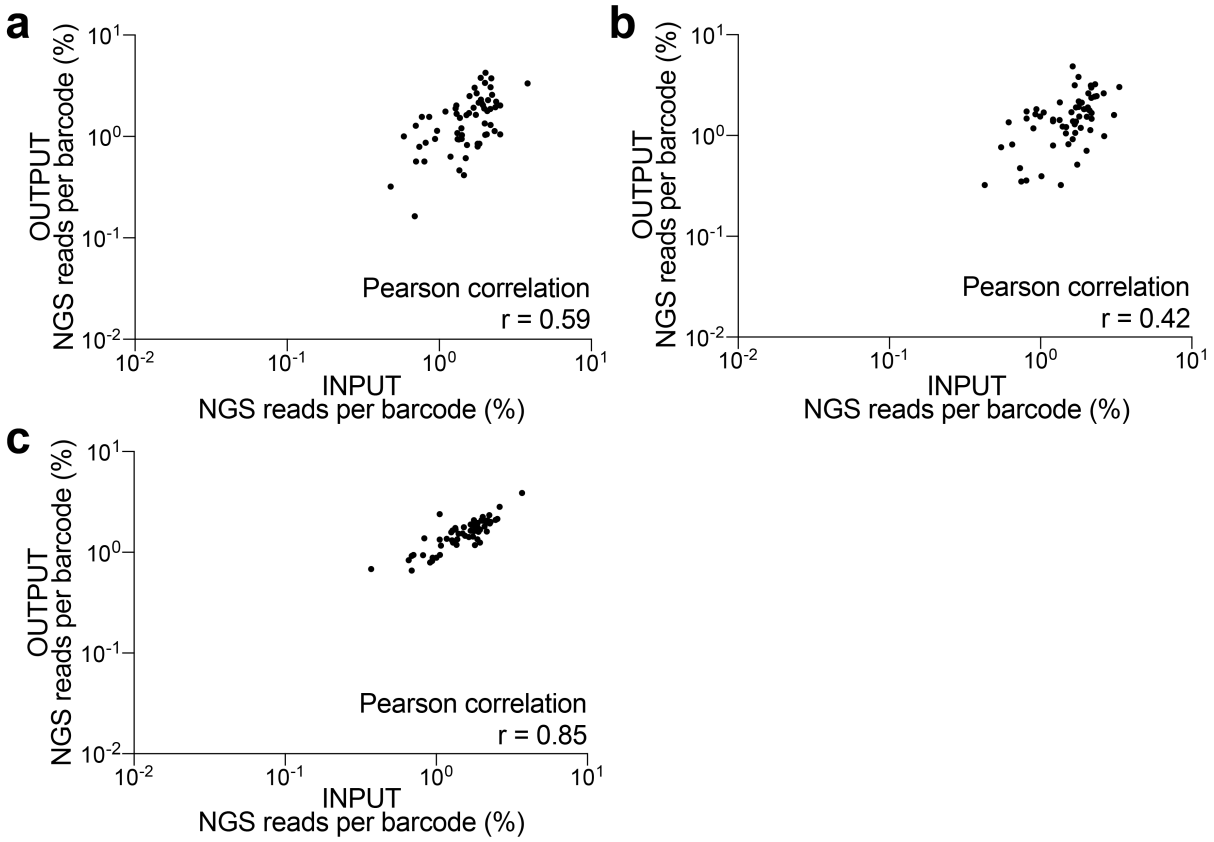

651

652

653 **Figure S4: Assessment of *in vivo* stability of barcoded libraries of parasites.** Three separate inoculums of
654 the same complex barcode library pool were injected intraperitoneally into mice, allowed to grow for 36
655 hours, and then retrieved. Scatter plots present data for the percentage representation of individual barcodes
656 within the library pools for parasite infection inoculums (INPUT) compared with the corresponding
657 population retrieved from the peritoneal cavity of the infected host (OUTPUT) for (**a**) 0.25×10^6 parasites,
658 PCC r = 0.59, n = 62, P (two-tailed) = <0.0001. **b**) 0.5×10^6 parasites, PCC r = 0.62, n = 62, P (two-tailed) =
659 0.0006. **c**) 1×10^6 parasites, PCC r = 0.85, n = 62, P (two-tailed) = <0.0001. PCC values provided on scatter
660 plots indicate degree of correlation between populations being compared.

661

662

663

664

665

666

667 **Figure S5**

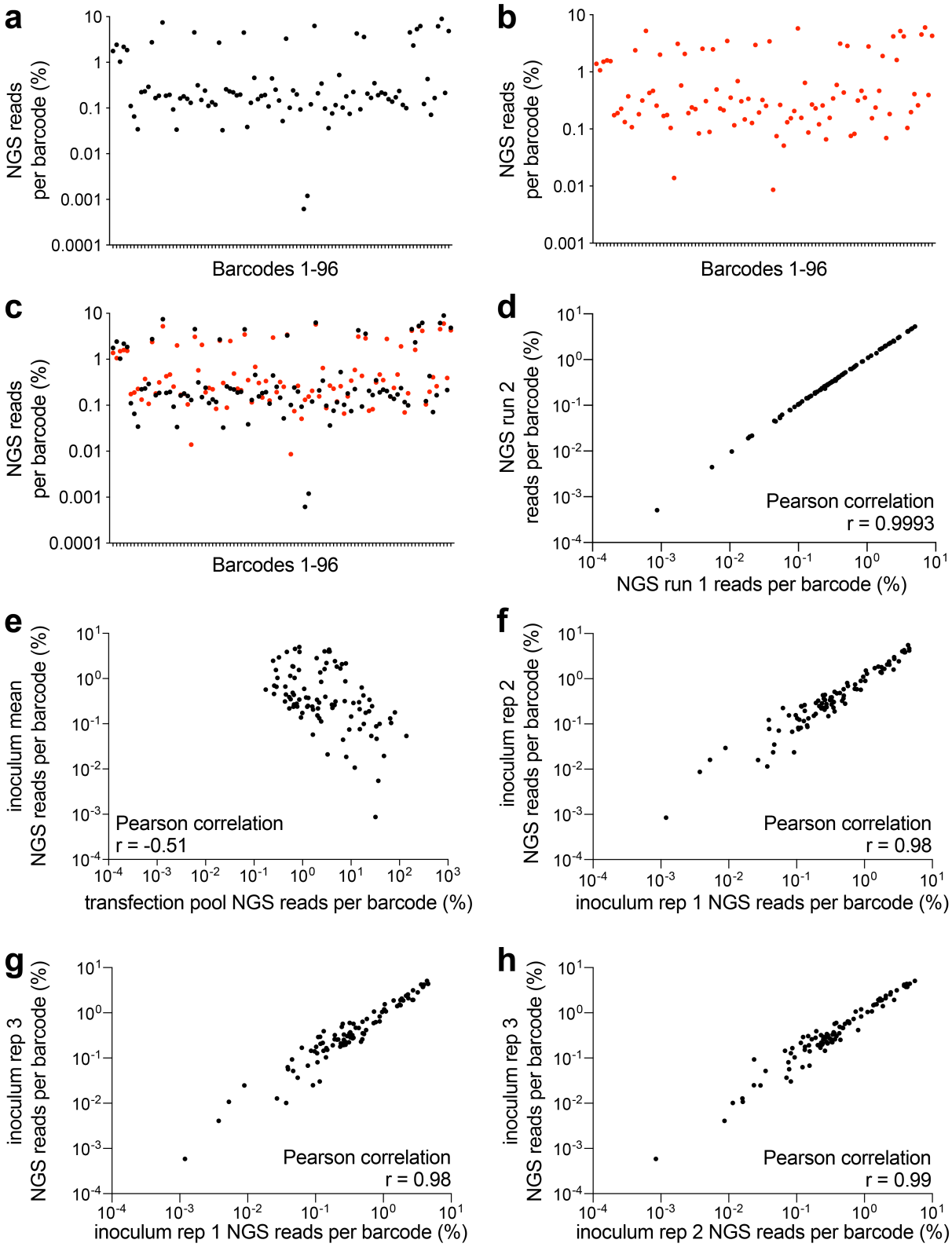

668

669

670 **Figure S5: Analysis of molecularly barcoded *T. gondii* libraries generated using a one-pot transfection**

671 **approach.** One-pot transfections using (**a**) RHΔ*ku80* or (**b**) PruΔ*ku80* yield a complex library of barcoded

672 strains with complete representation of all 96 oligos included in the transfection pool. **c**) Overlay of data

673 from the different strain transfections (**b** and **c**). Scatter plots in **a-c** present relative percentage frequency of
674 barcodes within the population, distributed according to barcode identifier (1-96). **d**) Scatter plot of relative
675 percentage frequency of barcodes within a single genomic sample, processed on independent NGS runs.
676 PCC r = 0.99, n = 96, P (two-tailed) = <0.0001. **e-h**) Scatter plots comparing relative percentage frequency
677 of barcode for the one-pot transfection pool versus the expanded inoculum mean (**e**) PCC r = -0.50, n = 96, P
678 (two-tailed) = <0.0001, and comparison of each of the three independently *in vitro*-expanded biological
679 replicates of the inoculum used for the mouse infection (**f**) PCC r = 0.98, n = 96, P (two-tailed) = <0.0001;
680 (**g**) PCC r = 0.98, n = 96, P (two-tailed) = <0.0001; (**h**) PCC r = 0.99, n = 96, P (two-tailed) = <0.0001. PCC
681 values provided on scatter plots indicate degree of correlation between populations being compared.
682